Optics and Lasers in Engineering 49 (2011) 507–513

Contents lists available at ScienceDirect

Optics and Lasers in Engineering

journal homepage: www.elsevier.com/locate/optlaseng

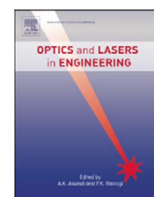

# Development and construction of rotating polarizer analyzer ellipsometer

Taher M. El-Agez, Sofyan A. Taya *

*Physics Department, Islamic University of Gaza, P.O. Box 108, Gaza, Palestinian Authority*

ARTICLE INFO

*Article history:*
Received 6 November 2010
Received in revised form
6 December 2010
Accepted 5 January 2011

*Keywords:*
Ellipsometry
Rotating polarizer analyzer ellipsometer
Optical properties of Au
ZnSe
$SiO_2$

ABSTRACT

A detailed mathematical derivation and an experimental characterization of one to two ratio rotating polarizer analyzer ellipsometer (RPAE) are presented. The alignment, calibration, and testing of reference samples are also discussed. The optical properties of some known materials obtained by the proposed ellipsometer will be shown and compared to accepted values. Moreover, the constructed ellipsometer will be tested using two ellipsometry standards with different thicknesses.

© 2011 Elsevier Ltd. All rights reserved.

## 1. Introduction

Ellipsometry in different forms has been studied for several centuries [1–5]. The most general meaning of ellipsometry is the measurement and analysis of elliptical polarization of light. Recently, ellipsometry has been studied extensively as a non-destructive technique for characterization of bulk solids and thin films. It is a very powerful technique since it overcomes two major problems that other reflectance measurement techniques suffer. In ellipsometry, phase is measured directly and is not calculated by the Kramers–Kronig method which involves extrapolations. Moreover, ellipsometric measurements are relatively insensitive to intensity fluctuations of the light source and macroscopic roughness. Scattered light by macroscopic rough surface is a serious problem in reflectometry but not in ellipsometry, for which absolute intensity measurements are not required. An ellipsometer measures the change in polarization state of incident light. If linearly polarized light of known orientation is reflected from a surface, then the reflected light will be elliptically polarized. The shape and orientation of the ellipse depend on the angle of incidence, the direction of the polarized incident light, and the reflection properties of the surface. Two parameters $\psi$ (the ratio of reflection coefficients) and $\Delta$ (phase change between p- and s-polarized lights) are determined in one single ellipsometric measurement. This makes it possible to obtain both the real and imaginary parts of the complex dielectric function of a homogeneous material. For a reflecting surface, the forms of $\Delta$ and $\psi$ are

$$\Delta=\delta_p-\delta_s \text{ and } \tan\psi=\frac{|r_p|}{|r_s|}, \tag{1}$$

where $\delta_p$ and $\delta_s$ are the phase changes for the p and s components of light and $r_p$ and $r_s$ are the complex Fresnel reflection coefficients for the p and s components, respectively, which may be written as

$$\left.\begin{aligned} r_p&=\rho_p e^{i\delta_p}\\ r_s&=\rho_s e^{i\delta_s}\end{aligned}\right\}. \tag{2}$$

The expressions for $r_p$ and $r_s$ for a single interface between medium 0 (ambient), with a complex refractive index $N_0$, and medium 1 (substrate), with a complex refractive index $N_1$ are given by [1]

$$r_p=\frac{N_1\cos\theta_0-N_0\cos\theta_1}{N_1\cos\theta_0+N_0\cos\theta_1}, \tag{3}$$

$$r_s=\frac{N_0\cos\theta_0-N_1\cos\theta_1}{N_0\cos\theta_0+N_1\cos\theta_1}, \tag{4}$$

where $\theta_0$ and $\theta_1$ are the angles of incidence and refraction, respectively.

Early in the 1970s, the dynamic scanning ellipsometer showed a great ability for determining optical constants of materials in the range 1.5–6 eV photon energy [6,7]. Since then, ellipsometry has received an increasing interest and the technique has been improved. Different models that can work in the visible region have been proposed and constructed [8–12]. Among the various configurations of spectroscopic ellipsometers commonly used is

* Corresponding author. Tel.: +972 8 2823311x2620; fax: +972 8 2860800.
*E-mail addresses:* telagez@iugaza.edu.ps (T.M. El-Agez), staya@iugaza.edu.ps (S.A. Taya).

0143-8166/$ - see front matter © 2011 Elsevier Ltd. All rights reserved.
doi:10.1016/j.optlaseng.2011.01.005

the rotating analyzer ellipsometer (RAE) [6]. In such a model, the polarizer angle $P$ is fixed while the analyzer angle $A$ rotates at an angular speed $\omega$. In terms of $A=\omega t$, the intensity of light emerging from the analyzer can be written as one dc and two ac components, from which the ellipsometric parameters $\psi$ and $\Delta$ are obtained. RAE has the advantage of simple system design but it involves the dc component, which causes a serious problem. The reduction of dc background requires particular techniques and the calibration of a such system is also time-consuming [10]. In 1987, a RPAE was proposed and constructed [10]. In the design, the polarizer and the analyzer rotate at a speed ratio 1:2. The final light intensity then contains three cosine terms, from which $\psi$ and $\Delta$ are calculated. In this design, the errors arising from the phase shift and dc background are eliminated. An improved RPAE was proposed [11,12] with the speed ratio still being 1:2 but with the incident angle being fully variable. Moreover, a fixed polarizer was placed in the optical path to eliminate the source polarization effect. The final light intensity thus contains four ac components. The optical constants and the ellipsometric parameters were obtained by calculating any one of the two sets of ac signals. In 2010, El-Agez et al. [13] proposed a novel type of spectroscopic ellipsometer in which the polarizer and the analyzer rotate synchronously in opposite directions at the same speed. The light intensity involves four components, one dc and three cosine terms, with frequencies $\omega$, $2\omega$, and $3\omega$.

In this work, we describe the same structure presented in [10–12], in which the polarizer and the analyzer rotate in the same direction at a ratio 1:2 with additional developments. First, we developed the theoretical analysis presented in [10–12] to show that the Fourier transform of intensity contains nine components, one dc and eight ac. These coefficients will be derived in details. For a specific alignment of the elements comprising the structure, we show that the number of coefficients reduces to five, one dc and four ac. Second, we show that the ellipsometric parameters as well as the optical constants can be obtained by calculating any one of four sets of ac signals. The extraction of the optical constants of the sample under test from these coefficients will be presented. The experimental part in [10–12] was restricted to the characterization of Au only. In our work, the optical properties of Au, ZnSe, and $SiO_2$ obtained by the proposed ellipsometer will be shown. The experimental results will be compared to accepted values. Moreover, the constructed ellipsometer will be tested using two ellipsometry standards with different thicknesses.

## 2. Theory

Assume that a cascade of $m$ optical devices is introduced in the path of monochromatic wave of an incident electric field $E_i$. Let $T_i$ be the Jones transmission matrix of the $i$th element; then the transmitted electric field will be

$$E_t = T_m T_{m-1} T_{m-2} \cdots T_1 T_0 E_i. \tag{5}$$

Consider unpolarized monochromatic light passing through a fixed polarizer that then passes through a rotating polarizer with angular speed $\omega$. The light reflects from the surface of a sample under test. Finally, the reflected light passes through another rotating analyzer to a detector as shown in Fig. 1. Assume that the transmission axis of the fixed polarizer makes an angle $\theta$ with respect to the plane of incidence. Let $P$ be the angle between the transmission axis of the rotating polarizer and the plane of incidence at any moment and $A$ be that for the rotating analyzer at any moment. Also, consider the case of oblique reflection from the interface between two isotropic materials. If all the optical elements are presumed to be ideal, according to Eq. (5) the

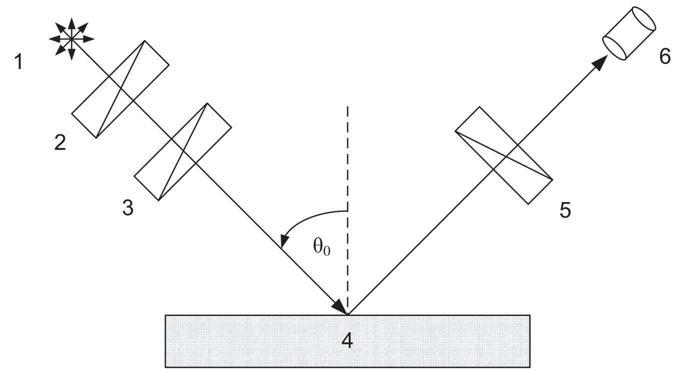


**Fig. 1.** Schematic illustration of the RPAE under consideration: (1) unpolarized light, (2) fixed linear polarizer, (3) linear polarizer rotating at $\omega$, (4) isotropic sample, (5) linear analyzer rotating at $2\omega$, and (6) detector.

transmitted electric field of the system described above will be

$$E_t = \begin{bmatrix} \cos^2 A & \sin A\cos A \\ \sin A\cos A & \sin^2 A \end{bmatrix} \begin{bmatrix} r_p & 0 \\ 0 & r_s \end{bmatrix} \begin{bmatrix} \cos^2 P & \sin P\cos P \\ \sin P\cos P & \sin^2 P \end{bmatrix} \begin{bmatrix} \cos\theta \\ \sin\theta \end{bmatrix} E_i. \tag{6}$$

The light signal received by the detector is given by

$$I \propto |E_t|^2 = \left[\frac{M\sigma_1}{2} + \frac{N\sigma_2}{2} + \rho_s\rho_p\sigma_3\cos\Delta\right][1+\cos 2(P-\theta)], \tag{7}$$

where

$$\sigma_1 = \cos(2A)+\cos(2P), \tag{8}$$

$$\sigma_2 = 1+\cos(2A)\cos(2P), \tag{9}$$

$$\sigma_3 = 1+\sin(2A)\sin(2P), \tag{10}$$

$$N = \rho_s^2+\rho_p^2, \tag{11}$$

$$M = \rho_s^2-\rho_p^2. \tag{12}$$

The amplitudes of the reflection coefficients in terms of $M$ and $N$ are

$$\rho_s = \sqrt{\frac{N+M}{2}}, \tag{13}$$

$$\rho_p = \sqrt{\frac{N-M}{2}}. \tag{14}$$

In the one to two ratio rotating polarizer/analyzer technique, the analyzer rotates twice as fast as the polarizer. If $\delta$ and $\tau$ are the offset of the analyzer and polarizer at the starting point, respectively, then

$$P = \omega t+\tau, \tag{15}$$

$$A = 2\omega t+\delta. \tag{16}$$

The intensity at the detector in terms of the angular speed of the polarizer will be

$$I(t) = a_0 + \sum_{n=1}^{4} a_n\cos 2n\omega t + \sum_{n=1}^{4} b_n\sin 2n\omega t, \tag{17}$$

where the $a$-terms are the even coefficients of the Fourier spectrum and they are written as

$$a_0 = \frac{N}{2}\left[1+\frac{\cos 2(\delta-2\tau+\theta)}{2}\right] + \frac{M}{2}\cos 2(\theta) + \frac{\rho_s\rho_p\cos\Delta[\cos 2(\delta-2\tau+\theta)]}{2}, \tag{18}$$

$$a_1 = N\left[\frac{\cos 2(\delta-\tau)}{4}+\frac{\cos 2(\tau-\theta)}{2}\right]+M\left[\frac{\cos 2(\tau)}{2}+\frac{\cos 2(\delta-\tau+\theta)}{4}\right] + \frac{\rho_s\rho_p\cos\Delta\cos 2(\delta-\tau)}{2}, \tag{19}$$

$$a_2 = \frac{N}{8}\left[\cos 2(\delta-\theta)+\cos 2(\delta+\theta)\right]+\frac{M}{2}\left[\cos 2(\delta)+\frac{\cos 2(2\tau-\theta)}{2}\right] + \frac{\rho_s\rho_p\cos\Delta[\cos 2(\delta-\theta)-\cos 2(\delta+\theta)]}{4}, \tag{20}$$

$$a_3 = \frac{N\cos 2(\delta+\tau)}{4}+\frac{M\cos 2(\delta+\tau-\theta)}{4}-\frac{\rho_s\rho_p\cos\Delta\cos 2(\delta+\tau)}{2}, \tag{21}$$

and

$$a_4 = \left[\frac{N}{8}-\frac{\rho_s\rho_p\cos\Delta}{4}\right]\cos 2(\delta+2\tau-\theta). \tag{22}$$

The $b$-terms are the odd coefficients and they are written as

$$b_1 = -N\left[\frac{\sin 2(\delta-\tau)}{4}+\frac{\sin 2(\tau-\theta)}{2}\right]-M\left[\frac{\sin 2(\tau)}{2}+\frac{\sin 2(\delta-\tau+\theta)}{4}\right] - \frac{\rho_s\rho_p\cos\Delta\sin 2(\delta-\tau)}{2}, \tag{23}$$

$$b_2 = -\frac{N}{8}\left[\sin 2(\delta-\theta)+\sin 2(\delta+\theta)\right]-\frac{M}{2}\left[\sin 2(\delta)+\frac{\sin 2(2\tau-\theta)}{2}\right] - \frac{\rho_s\rho_p\cos\Delta[\sin 2(\delta-\theta)-\sin 2(\delta+\theta)]}{4}, \tag{24}$$

$$b_3 = -\frac{N\sin 2(\delta+\tau)}{4}-\frac{M\sin 2(\delta+\tau-\theta)}{4}+\frac{\rho_s\rho_p\cos\Delta\sin 2(\delta+\tau)}{2}, \tag{25}$$

and

$$b_4 = \left[-\frac{N}{8}+\frac{\rho_s\rho_p\cos\Delta}{4}\right]\sin 2(\delta+2\tau-\theta). \tag{26}$$

A closer look at both even and odd coefficients of the fourth harmonics of the Fourier transform of intensity reveals an important relation that connects $\tau$, $\delta$ and $\theta$, namely

$$4\tau+2(\delta-\theta) = \tan^{-1}\left[\frac{-b_4}{a_4}\right]. \tag{27}$$

This formula is true regardless of the sample used or the angle of incidence. Thus it is a property of the system that is mainly determined by the relative positions of the three polarizers.

Assuming that the azimuth angles $\theta$, $\tau$, and $\delta$ are equal to zero, the odd coefficients are all zero and the even ones are given by

$$a_0 = \frac{3}{4}N+\frac{1}{2}M+\frac{1}{2}\rho_s\rho_p\cos\Delta, \tag{28}$$

$$a_1 = \frac{3}{4}N+\frac{3}{4}M+\frac{1}{2}\rho_s\rho_p\cos\Delta, \tag{29}$$

$$a_2 = \frac{1}{4}N+\frac{3}{4}M, \tag{30}$$

$$a_3 = \frac{1}{4}N+\frac{1}{4}M-\frac{1}{2}\rho_s\rho_p\cos\Delta, \tag{31}$$

and

$$a_4 = \frac{1}{8}N-\frac{1}{4}\rho_s\rho_p\cos\Delta. \tag{32}$$

The ellipsometric parameters $\psi$ and $\Delta$ can be obtained using any set containing three coefficients. Without depending on $a_0$, we have four sets, namely, ($a_1$, $a_2$, $a_3$), ($a_1$, $a_2$, $a_4$), ($a_1$, $a_3$, $a_4$), and ($a_2$, $a_3$, $a_4$). $\psi$ and $\Delta$ can be determined as follows:

$$\tan\psi_{123} = \sqrt{\frac{a_1+a_3}{2a_1-4a_2+2a_3}}, \tag{33}$$

$$\cos\Delta_{123} = \frac{a_1-3a_3}{\sqrt{(a_1+a_3)(2a_1-4a_2+2a_3)}}, \tag{34}$$

$$\tan\psi_{124} = \sqrt{\frac{2a_1+a_2+4a_4}{4a_1-7a_2+8a_4}}, \tag{35}$$

$$\cos\Delta_{124} = \frac{3(a_1-a_2-4a_4)}{\sqrt{(2a_1+a_2+4a_4)(4a_1-7a_2+8a_4)}}, \tag{36}$$

$$\tan\psi_{134} = \sqrt{\frac{a_1+a_3}{a_1-7a_3+16a_4}}, \tag{37}$$

$$\cos\Delta_{134} = \frac{a_1-3a_3}{\sqrt{(a_1+a_3)(a_1-7a_3+16a_4)}}, \tag{38}$$

$$\tan\psi_{234} = \sqrt{\frac{a_2-2a_3+4a_4}{a_2-4a_3+8a_4}}, \tag{39}$$

$$\cos\Delta_{234} = \frac{a_2-3a_3+4a_4}{\sqrt{(a_2-2a_3+4a_4)(a_2-4a_3+8a_4)}}, \tag{40}$$

## 3. Experimental work

The main components of RPAE are shown in Fig. 2. The following is a description of each component:

1. A 0.95 mW Helium–Neon (spectra physics model 155) laser is used mainly to adjust the position and the height of all the optical parts.
2. A reference pinhole with outside diameter of 1 mm is used to make sure that the height of the laser beam is fixed at a certain height from the surface of the table.
3. A front surface mirror is used to reflect the laser beam towards the beam splitter.
4. A 50 W and 12 V quartz halogen tungsten lamp is used as the light source of the ellipsometer.
5. A compound lens assembly with a small *F*# of 1.6 is used to collect the largest amount of light. The filament is placed at the front focal point of this lens assembly to produce nearly parallel beam.
6. A double convex lens with a focal length of +24 cm is used to focus light at the entrance slit of the monochromator.
7. An aperture stop is used to limit the size of the maximum cone of light seen by an axial point at the slit. This stop serves to match the *F*# of the light source with that of the monochromator.
8. A Perkin-Elmer monochromator model E1 with *F*# 7 is used to obtain semi-monochromatic light.
9. A double convex lens with focal length +16 cm is used to collect light from the monochromator and focus it to the pinhole.
10. Reference pinhole with outside diameter of 1 mm is used to make sure that the height of the light beam is fixed at a certain height from the surface of the table.
11. A double convex lens with focal length equal to +20 cm is used. The pinhole (item 10) is placed at the focal point of this

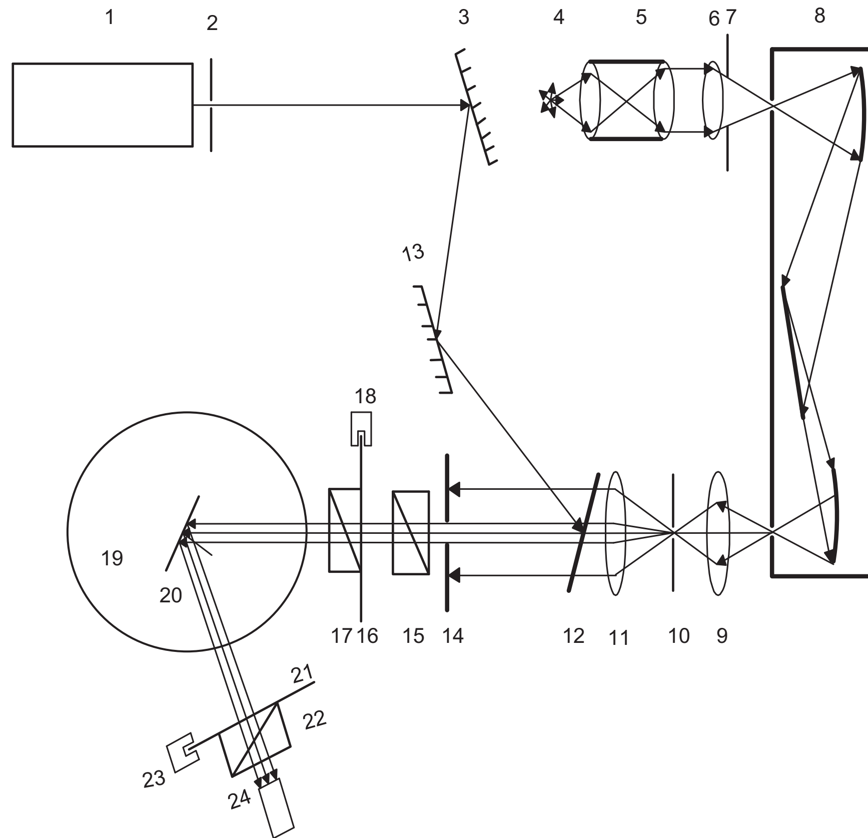


**Fig. 2.** Schematic diagram of the homemade ellipsometer under consideration.

lens such that the emerging beam will be nearly parallel. The lens is mounted on a *x–y–z* stage driven with micrometers.

12. Pellicle beam splitter is placed in the path of the laser beam such that the paths of both of the transmitted monochromatic beam and the reflected laser beam will coincide.
13. A front surface mirror that serves to reflect the laser beam to the beam splitter is used.
14. An aperture stop with outer diameter of 4 mm is placed in the path of both the monochromatic and the laser beams. It limits the size of the beam spot on the sample.
15. A Glan–Taylor ultra–violet prism polarizer model MGTYE10 made by Karl Lambrecht. It has a spectral range 214–2300 nm and $5\times10^{-6}$ extinction ratio.
16. A circular disk is attached to the barrel of the polarizer with a pinhole drilled near its edge to define the home position of the polarizer.
17. A polarizer identical to that described above is used. This polarizer can be rotated using two phase hybrid permanent magnet $1.8^{\circ}$ per step stepper motors. The motors are driven by an indexer–driver unit that receives 12,800 micro-steps per revolution from a PC through an RS232C cable.
18. Photo-gate is used to define the home position of the polarizer. The position of the gate can be finely adjusted using a micrometer attached to the photo-gate.
19. A rotating table is used to define the angle of incidence on the sample. The table is accurate within $\pm0.05^{\circ}$.
20. A sample holder is placed at the center of the table and is used to hold the sample under test. The holder can rotate about an axis perpendicular to the rotating table. Moreover, the tilt of the sample can be adjusted using three fine screws.
21. A circular disk is attached to the barrel of the analyzer with a pinhole drilled near its edge to define the home position of the analyzer.
22. Another prism polarizer as described in item 15 serves as an analyzer. It also can be rotated by computer driven indexer–driver unit as described before in item 17.
23. Photo-gate is used to define the home position of the analyzer. It can be finely adjusted using a micrometer.
24. A head on photomultiplier tube made by Hammatsu, model number R1464 with spectral range from 185 to 850 nm is used.

The rotating polarizer is adjusted first using the idea that the reflection of p-polarization undergoes a minimum at the Brewster's angle of incidence. Accordingly, the analyzer is aligned to the position where extinction is achieved (crossed polarizers). The following steps provide the details of such a process.

### 3.1. Alignment of the rotating polarizer

1. A certain wavelength is chosen (632.8 nm for example) and a reflecting surface like silica or silicon is chosen. Brewster's angle of this material is calculated at that wavelength and the angle of incidence is fixed at this value.
2. Reflected light is allowed to hit a movable photomultiplier tube connected to an oscilloscope as well as a data acquisition board hooked internally to a PC.
3. Rotate the polarizer by hand until the reading on the scope is at minimum.
4. Loosen the set screw on the circular disk (item 16) and rotate it by hand (with the polarizer still fixed in place) until the photo-gate (item 18) is activated. This is roughly the home position of the first rotating polarizer.
5. The stepper motors are activated and the polarizer is rocked by a small magnitude around the home position using the code written to control the motors. Data are collected and fitted to a

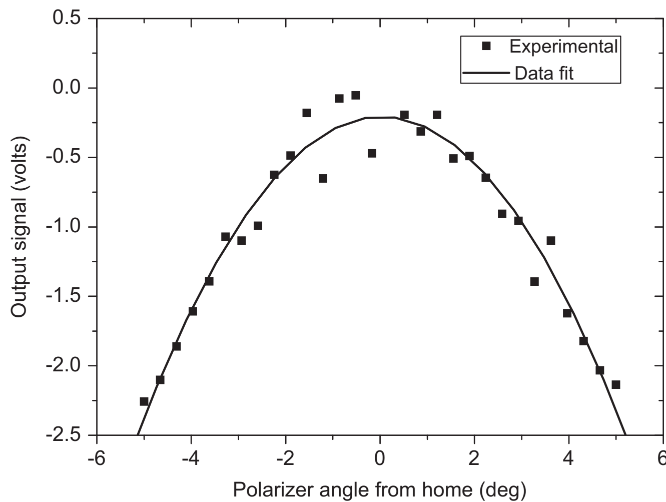


**Fig. 3.** Alignment of the rotating polarizer by rocking it around the home position.

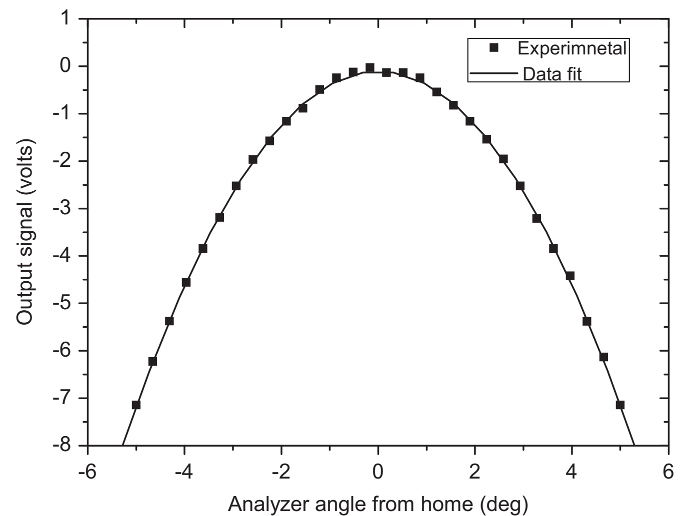


**Fig. 4.** Alignment of the analyzer by rocking it around the home position.

parabola. The angle error is calculated also using the computer. The error can be minimized to $\pm 0.01^\circ$ by fine positioning of the photo-gate using the attached micrometer. Fig. 3 shows a real example of data taken while rocking the polarizer and the best fit to a parabola.

### 3.2. Analyzer alignment

The home position of the analyzer is chosen to be the s-polarization state. The following steps describe the procedure to align the analyzer:

1. The first rotating polarizer is fixed at the p-state and the arm that supports the analyzer is rotated to the 180° position (straight through position with no sample)
2. The analyzer is rotated by hand to the point where the intensity of the detected signal is nearly zero.
3. Adjust the position of the circular disk (item 21) until the second photo-gate (item 23) is activated.
4. The analyzer is rocked by a small angle around that position and the collected data are fitted to a parabola. The micrometer on the photo-gate is fine-tuned for the minimum angle error. Fig. 4 shows a real experimental data and the fitted curve.

### 3.3. Alignment of the fixed polarizer

The azimuth angle of the fixed polarizer can be easily found using the Fourier transform of the signal in the straight through position (no sample). The angle will be given by

$$2\theta = \tan^{-1}\left[\frac{b_4}{a_4}\right] \tag{41}$$

Many measurements are done and the average is taken to minimize all kinds of errors.

## 4. Applications

One to two RPAE was used to study the optical properties of the following samples.

### 4.1. Air/gold interface

Data was taken at an angle of incidence of 75° on a flat uncoated front surface gold mirror purchased from Edmund Scientific (catalog number D41801). The wavelength used was varied from 440700 nm and the slit size of the monochromator was fixed at 5000 nm.

Calculations of the real and imaginary parts of the refractive index of the sample are based on the well-known equation [1]

$$\varepsilon = \sin^2\theta_0 + \sin^2\theta_0 \tan^2\theta_0 \left(\frac{1-\rho}{1+\rho}\right)^2, \tag{42}$$

where $\rho = r_p/r_s = \tan\psi\, e^{i\Delta}$, $\varepsilon = \varepsilon_1 + i\varepsilon_2$, $\tilde{n} = \sqrt{\varepsilon} = n + ik$, $\varepsilon_1 = n^2 - k^2$, and $\varepsilon_2 = 2nk$.

Results are compared with accepted values found in two references. First, values are given in the handbook of optical constants of solids [14]. These optical constants were reported by Theye [15] and were obtained by normal reflectance and transmittance from thin films (10–25 nm) of pure gold (99.99%). The second reference is that reported by Johnson and Christy [16]. Fig. 5 shows the values of the real and complex parts of refractive index of Au in the spectral range 440–700 nm. The discrepancy in optical properties between the reported values could be explained based on the sample preparation methods as well as the techniques used [17]. In general the values of $n$ match with those reported in the first reference while the $k$ values are in excellent agreement with the second source.

### 4.2. Zinc selenide (ZnSe)

The optical properties of ZnSe sample were studied in the spectral range 420–700 nm at 70° angle of incidence and were compared to published data for ZnSe [18]. The sample was polished using 1 μm aluminum oxide powder on one side while the other surface was roughened and tilted to prevent reflection from the back side of the sample. The polished sample showed lower $n$ values than the accepted values and higher $k$ values as shown in Fig. 6. This can be interpreted based on the surface damage (roughness) due to the polishing procedure. Surface roughness tends to lower the refractive index $n$ and increase the extinction coefficient. A rough surface with roughness on the order of the wavelength can be modeled as a discrete thin film whose thickness is equal to the root mean square (rms) value of the roughness on top of a smooth bulk material. The optical constants of such a thin film lie between those of air and those of the bulk material due to the presence of voids. The effective index can be estimated using the effective medium approximation assuming a mixture of bulk material and air. The overall impact

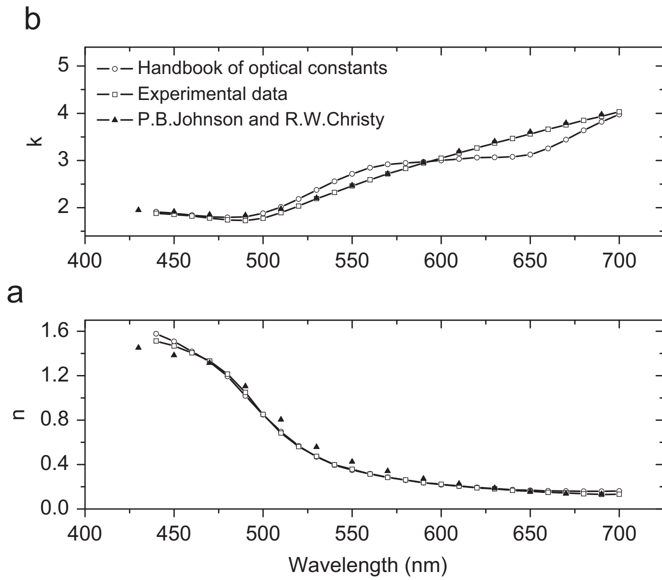


**Fig. 5.** Real part (a) and imaginary part (b) of the refractive index of gold versus wavelength.

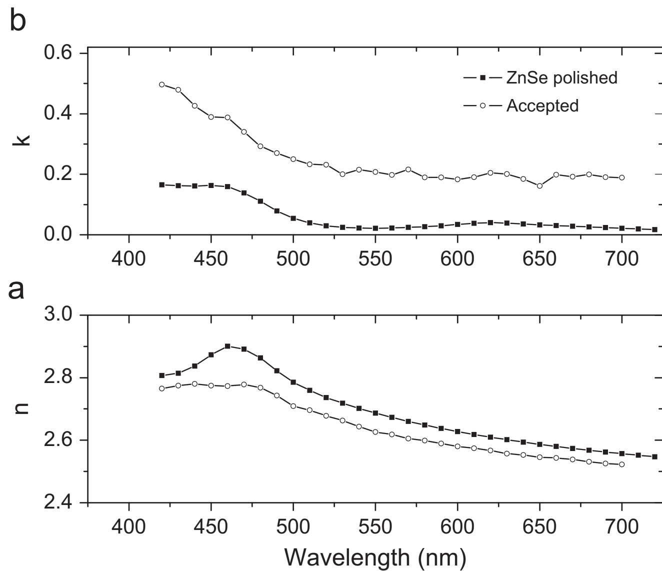


**Fig. 6.** Measured and the accepted values of the real part (a) and the imaginary part (b) of complex refractive index of ZnSe versus wavelength.

of such a film on the rough material is to lower the real part of the index and increase the absorption coefficient. On the other hand, very rough surface tends to cause depolarization of the reflected beam, which has striking impact on the measured ellipsometric parameters. This effect is very difficult to take into account or to model.

### 4.3. *Silicon native oxide*

A series of 25 measurements of Psi and Delta were taken on a blank silicon wafer at an angle of incidence of 75° and wavelength of 550 nm. The system is modeled as one thin film of the oxide on top of a silicon substrate. The average values of Psi and Delta were 3.81° and 134°, respectively. Locating these values on the Psi–Delta trajectory shown in Fig. 7 reveals a native oxide layer of average thickness $3.5\pm1$ nm, which agrees with the values reported by Jacob [19] and Vuye et al. [20].

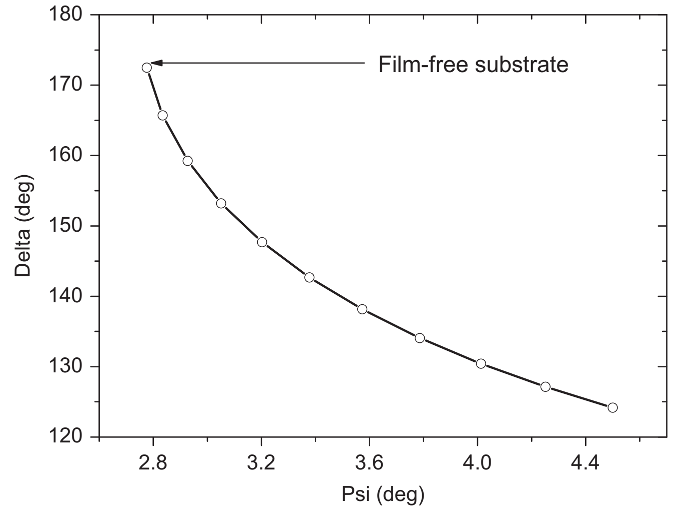


**Fig. 7.** Psi–Delta trajectory for 5 nm thin film (in 0.5 nm increments) of $SiO_2$ on Si wafer at wavelength of 550 nm and 75° angle of incidence.

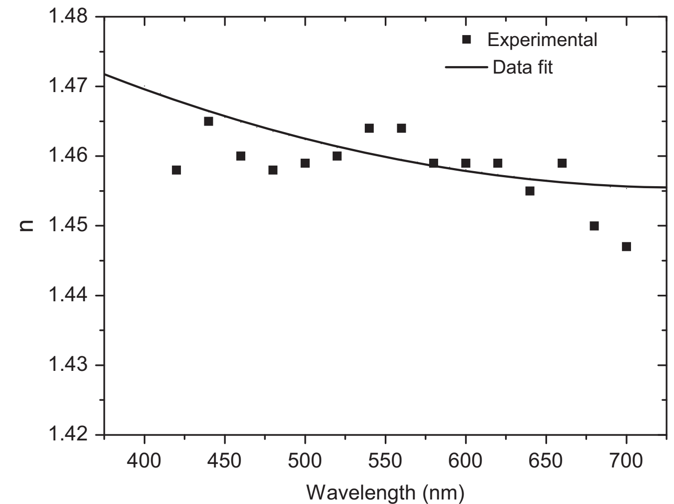


**Fig. 8.** Measured values of the index of silicon dioxide thin film on silicon wafer as a function of wavelength for ellipsometry standard 1.

### 4.4. *Ellipsometry standards*

Two ellipsometry standards made by Rudolph Research (A11188) were investigated at 632.8 nm as well as in the spectral range 420–700 nm. Each one of these standards is a silicon wafer of 3-in. outer diameter coated with a fairly uniform film of silicon dioxide. The following are the detailed results from the two samples. The first wafer is coated with thin film of thickness $46\pm0.3$ nm and has a refractive index of 1.462 at 632.8 nm. Measurements were taken at 75° angle of incidence and 632.8 nm. The measured index was 1.46 with percentage error of $-0.137\%$ and the measured thickness was 47.1 nm with percentage error of 2.46%. Moreover, the spectroscopic measurements of refractive index of the film in the spectral range 420–700 nm are shown in Fig. 8.

The second wafer is coated with silicon dioxide film of thickness $117.1\pm0.3$ nm and has a refractive index of $1.462\pm0.002$ at wavelength of 632.8 nm. Experimental data were taken at 70° angle of incidence and wavelength of 632.8 nm. The measured index was 1.463 with percentage error of 0.068% and the measured thickness

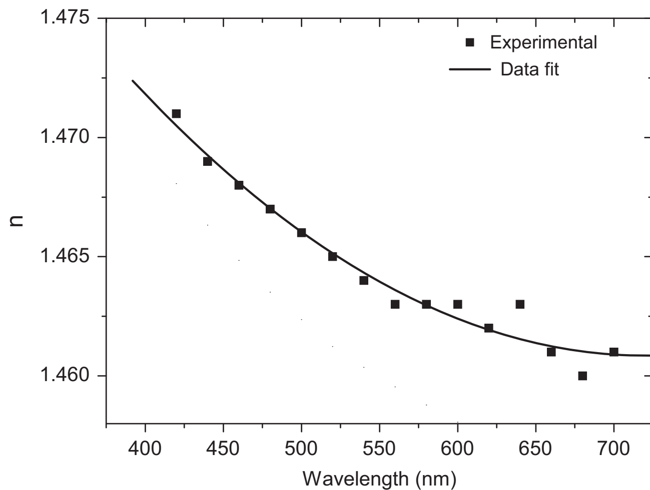


**Fig. 9.** Measured values of the index of silicon dioxide thin film on silicon wafer as a function of wavelength for ellipsometry standard 2.

was 117.8 nm with percentage error of 0.6%. The spectroscopic measurements of refractive index of the film in the spectral range 420–700 nm are shown in Fig. 9.

## 5. Conclusion

We have constructed one to two ratio rotating polarizer analyzer photometric ellipsometer.

The mathematical analysis of the proposed RPAE is shown in detail. The components of the RPAE and their functions are described. The optical properties of some known materials were obtained experimentally and compared to accepted values. It has been proven from all cases studied above that the constructed RPAE is very sensitive to such a degree that it is able to detect the native oxide on silicon wafer. In general, the results obtained on various reflecting systems a in agreement with accepted values.

## References

[1] Azzam RM, Bashara NM. Ellipsometry and polarized light. Amsterdam: North-Holland; 1977.
[2] Hauge PS. Recent developments in instrumentation in ellipsometry. Surf Sci 1980;96:108–40.
[3] Woollam JA, Snyder PG, Rost MC. Variable angle spectroscopic ellipsometry: a non-destructive characterization technique for ultrathin and multilayer materials. Thin Solid Films 1988;166:317–23.
[4] Vedam K. Spectroscopic ellipsometry: a historical overview. Thin Solid Films 1998;313–314:1–9.
[5] Aspnes DE. Expanding horizons: new developments in ellipsometry and polarimetry. Thin Solid Films 2004;455–456:3–13.
[6] Aspnes DE. Fourier transform detection system for rotating analyzer ellipsometers. Opt Commun 1973;8:222–5.
[7] Aspnes DE. High precision scanning ellipsometer. Appl Opt 1975;14:220–8.
[8] Zaghloul AR, Azzam RM. Single-element rotating polarizer ellipsometer: psi meter. Surf Sci 1980;96:168–73.
[9] Vina L, Umbatch C, Cardona M, Vodopyanov L. Ellipsometric studies of electric interband transitions in $Cd_xHg_{1-x}Te$. Phys Rev B 1984;29:6752–60.
[10] Chen LY, Lynch DW. Scanning ellipsometer by rotating polarizer and analyzer. Appl Opt 1987;26:5221–8.
[11] Chen LY, Feng XW, Su Y, Ma HZ, Qian Y. Improved rotating analyzer–polarizer of scanning ellipsometer. Thin Solid Films 1993;234:385–9.
[12] Chen LY, Feng XW, Su Y, Ma HZ, Qian Y. Design of a scanning ellipsometer by synchronous rotation of the polarizer and analyzer. Appl Opt 1994;33:1299–305.
[13] El-Agez TM, El Tayyan AA, Taya SA. Rotating polarizer–analyzer scanning ellipsometer. Thin Solid Films 2010;518:5610–4.
[14] Palik ED. Handbook of optical constants of solids II. San Diego: Academic Press; 1991.
[15] Theye ML. Investigation of the optical properties of Au by means of thin semitransparent films. Phys Rev B 1970;2:3060–78.
[16] Johnson PB, Christy RW. Optical constants of the noble metals. Phys Rev B 1972;6:4370–9.
[17] Aspnes DE, Kinsborn E, Bacon DD. Optical properties of Au: sample effects. Phys Rev B 1980;21:3290–9.
[18] Jellison Jr. GE. Optical functions of GaAs, GaP, and Ge determined by two-channel polarization modulation ellipsometry. Opt Mater 1992;1:151–60.
[19] Jacob W. Surface reactions during growth and erosion of hydrocarbon films. Thin Solid Films 1998;326:1–42.
[20] Vuye G, Fisson S, Van VN, Wang Y, Rivory J, Abelès F. Temperature dependence of the dielectric function of silicon using in situ spectroscopic ellipsometry. Thin Solid Films 1993;233:166–70.